Supporting Information

Mulliken *et al.* 10.1073/pnas.0802602105

SI Text

Peak Mutual Information as a Function of Optimal Lag Time. Fig. S1 *A* and *B* plots the peak mutual information that each cell encoded for movement angle at its OLT, for both the center-out and obstacle tasks. First, notice that the center-of-mass values, −6 ms and 15 ms, for the center-out and obstacle distributions, respectively, were consistent with the median OLTs reported in Fig. 3*B*. This was, of course, due largely to the higher proportion of cells' having OLTs near 0 ms as illustrated in Fig. 3*B* but also to the larger amount of information encoded by neurons with OLTs close to zero lag, as mentioned in the main text. Specifically, during the center-out task, clearly forward-estimating neurons' (0 ms $\leq$ OLT $\leq$ 60 ms) mutual information was 0.043 $\pm$ 0.04 compared with 0.036 $\pm$ 0.03 for movement-angle neurons with other OLTs (OLT ≤ -30 ms, or, OLT $\geq$ 90 ms). Similarly, for the obstacle task, the average peak information of clearly forward-estimating neurons was 0.043 $\pm$ 0.03, whereas it was 0.034 $\pm$ 0.03 for movement-angle neurons with other OLTs.

Example STTFs and TEFs. Several additional example movement-angle STTFs and TEFs containing a variety of tuning strengths and OLTs are shown in Fig. S2.

Residual Tuning Significance Testing. To test for significance of tuning for angle (movement or goal), we subtracted the bootstrap distribution of surrogate TEFs from the bootstrap distribution of actual TEFs. A cell was initially considered significantly tuned and selected for further analysis if, at any lag time, 95% of these difference values were significantly >0. However, as mentioned in the main text, movement angle and goal angle may be correlated to various degrees depending on trajectory curvature (i.e., center-out task vs. obstacle task). Therefore, to control for the possibility that a cell's tuning for one angle is due entirely to tuning for the other angle, we performed an additional analysis to calculate the residual information encoded about the movement angle independent of the goal angle, and vice versa, as follows:

For each lag time, to test for significant tuning for movement angle, independent of goal angle, we randomly shuffled firing-rate samples that belonged to the same angle bin of a goal-angle tuning curve, effectively re-pairing firing rate samples with other goal angles from the same angle bin. Clearly, such a permutation would not affect the tuning for goal angle because firing rates were merely re-paired with their original corresponding goal angle. However, shuffling the firing-rate indices according to goal angle could affect the movement-angle tuning. In fact, movement-angle tuning would not be affected by permutation if and only if the goal angle and movement angle were identical during our tasks (i.e., perfect correlation). Alternatively, if movement angle and goal angle were completely uncorrelated (i.e., zero correlation), then permutation should corrupt the tuning for movement angle entirely. However, because goal and movement angles were partially correlated in our tasks, we observed instead that tuning strength for movement angle decreased after permutation of the firing-rate samples. Therefore, any decrease in the movement-angle mutual information that resulted from shuffling represented information that the cell encoded about movement angle and not the goal angle. If this difference, which we refer to as the residual movement-angle information, was significantly larger than its null hypothesis (generated in an analogous manner, but using surrogate spike trains) for any lag time, then the cell was considered to significantly encode movement angle, independent of its tuning for goal angle. If not, then it was unclear whether the cell encoded movement angle, and it was excluded from the movement angle population. Fig. S3 shows two different examples of cells' residual TEFs, one which was significantly larger than its residual null hypothesis (Fig. S3*A*) and another which was not (Fig. S3*B*). An analogous procedure was used to assess residual tuning for goal angle. Note, we computed the residual TEF only to ensure that movement-angle tuning could not be trivially explained by its correlation with goal angle. Importantly however, for OLT analysis, we did not use the residual TEF but instead used the full TEF described initially because it is possible that movement-angle tuning could be a function of an interaction between movement angle and goal angle, which the residual tuning measure does not reflect.

Neural Stationarity. It is important to show that the neural activity we measured was stationary over the time period for which we calculated mutual information. Therefore, we evaluated the stationarity of a neuron's firing rate during a trial and over an experimental session, similar to the approach taken by Paninski and colleagues (1).

First, we analyzed trends in the firing rate over the course of a session. The average firing rate was computed for each trial in a session, and the resulting trend in firing rate over the course of that session was fit by a line. The slope of the line and the percentage change in the firing rate across the session (from beginning to end) were derived from this fit. For consistency with the literature, we used the criteria of Paninski and colleagues to determine neural stationarity: if a cell's firing rate changed by <20% during the session "or" if the slope of the line fit was not significantly different from zero, the cell was deemed stationary. If both criteria failed to be met, an additional tuning analysis was performed to determine whether the actual STTF of the neuron changed significantly over the course of the session. To do this, we divided the experiment into two parts and constructed the STTF and pseudo-STTFs for both the first (A) and second (B) halves of the session. Bootstrap Monte Carlo resampling methods were used to generate a distribution of STTFs in the same manner as before. To quantify a change in tuning, we calculated the sum of squared differences between the bin values in $STTF_B$ and $STTF_A$ matrices as well as for the surrogate matrices, S_STTF_B and S_STTF_A. If the sum of the squared difference between the actual STTFs was >95% of the surrogate sum of squared differences, the cell was considered nonstationary and was excluded from the population. Using the above criteria, we found that the population was largely stationary; 220 of 221 and 168 of 170 movement-angle cells had stationary firing properties over the course of a session.

To analyze the intratrial stationarity of the firing rate, we aligned each trial to the reaction time and then computed the trial-averaged firing rate as a function of elapsed time. A line was fit to this trend, and the slope of the line and the percentage change in the firing rate were computed. To assess statistical significance of the mean trial slope, 100 bootstrap reshufflings were performed in which the firing rate time series was randomly shuffled, corrupting any trend in the firing rate over time but preserving its mean value. If the absolute value of the slope of the firing-rate trend was >95% of the bootstrap absolute-value slopes and the percentage change in the firing rate trend changed by >20%, the cell could be considered nonstationary. We found that 104 of 220 (47%) and 73 of 168 (44%) movement-angle

neurons, in the center-out and obstacle tasks, respectively, could be considered nonstationary based on this criteria. However, it unlikely that these intratrial firing-rate trends reflected any change that was related to the kinematics of the movement. First, any nonstationarity observed in the firing rate was not due to nonstationarity in the movement angle itself because the movement angle was almost always stationary over the course of the trial. Specifically, for 216 of 220 and 167 of 168 of the recorded sessions, the movement angle was determined to be stationary over the course of the trial based on the same criteria used above to assess intratrial neural stationarity. Moreover, we consistently observed cells that exhibited firing rate trends that increased for some trials and decreased for other trials under identical target conditions. Furthermore, simultaneously recorded cells frequently had opposite slopes for the same trial, also suggesting that any nonstationarity in the movement kinematics was not the cause of these trends in firing rate. Although it is possible that some of the cells we report on may also encode variables that we are not measuring or that are unrelated to the kinematics in our task, this does not limit the conclusions being drawn about correlations between neural activity and the movement angle.

Optimal Lag-Time Statistical Analysis. We performed an additional analysis to determine whether the mutual information encoded for movement angle at a cell's OLT was significantly larger than at all other lag times. Our null hypothesis was that the difference between the mutual information at the OLT and the mutual information at other lag times was not significantly different from zero. Bootstrapped values of mutual information at each lag time were subtracted from the mutual information at a cells' OLT. For each lag-time comparison, if 95% of these differences were >0, then the null hypothesis was rejected, and the mutual information at the OLT was concluded to be significantly larger than the mutual information encoded at the compared lag time. The outcome of all of these comparisons is summarized graphically in the 95% confidence OLT plots of Fig. S4, where horizontal error bars delineate the lag time range (30, 60, 90. . . ms) within which the OLT could be claimed to reside with at least 95% confidence. One hundred sixty of 220 (73%) and 154 of 168 (92%) of movement-angle neurons, for the center-out and obstacle tasks, respectively, have OLT confidence intervals <90 ms wide, suggesting that most neurons typically encode a strong dynamic estimate of the state of the movement angle. Note that we would not expect the temporal resolution of state-estimating neurons to consistently approach very small values due to implicit autocorrelation in the movement angle itself (movement-angle time constant <140 ms). Importantly however, over a variety of confidence-interval sizes (i.e., temporal resolutions), these plots show that the central tendency of the population was to consistently encode the recent, current, or upcoming state of the movement angle.

Finally, to control for the possibility that an autocorrelation present in the movement angle itself might contribute to the OLTs we observed, we also subtracted each surrogate TEF from its corresponding actual TEF and then recomputed the OLT for each surrogate-subtracted TEF in the population. As expected, because surrogate TEFs did not contain any temporal structure (e.g., Fig. 2*D* and Fig. S1 *B*, *D*, *F*, *H*, *J*, and *L*) and because firing rate and movement angle were stationary (see *Neural Stationarity*), this subtraction did not have any significant effect on the population OLT distributions. Indeed, a comparison of the OLT distributions before and after surrogate subtraction revealed that they were not statistically different ($P = 0.97$ and $P = 0.98$, for the center-out and obstacle tasks, respectively, Wilcox rank-sum test).

Last, note that OLT estimates for trajectories that contained less curvature (e.g., center-out task) will be, on average, more uncertain than OLTs reported for trajectories with more curvature, which contained richer changes in the movement angle (e.g., obstacle task). Therefore, the obstacle task may yield a more precise estimate of the shape of the OLT distribution. Consistent with this argument, we found that the variance of the obstacle OLT distribution was significantly less than the center-out OLT distribution ($P < 0.01$, median-subtracted Ansari–Bradley test). This tighter dispersion, combined with a forward shift in the median OLT for the obstacle task, resulted in an increase in the percentage of clearly forward-estimating movement-angle neurons for the obstacle task compared with the center-out task. Specifically, 88 of 220 (40%) and 94 of 168 (56%) neurons were clearly forward estimating, for the center-out and obstacle tasks, respectively.

Velocity Spatiotemporal-Encoding Analysis. To assess dynamic tuning of the movement state of the cursor, we chose to analyze the movement angle because (*i*) it could be fairly compared with the goal angle and (*ii*) of its close relationship to the full velocity vector (movement angle + speed), which has been reported to correlate most strongly with the firing intensity of primary muscle spindle afferents and has repeatedly been shown to correlate with movement-related activity in motor cortices, presumably involved in forming motor commands (1–7). As an additional control and for a more direct comparison with previous studies that have used velocity to represent the dynamic state of the hand, we also assessed the correlation of PPC neural activity with the state of the full velocity vector. When analyzing velocity tuning, movement angle was binned as before, but speed was discretized into five bins uniformly spaced across the full range of cursor speeds measured in a given session. In addition, when computing the mutual information between firing rate and velocity in Eq. **5**, the movement angle θ was replaced with the two-dimensional variable V, which consisted of both the direction and speed of the cursor. We found that the velocity OLT distributions were very similar to the movement-angle OLT distributions we reported. In particular, the distribution of OLTs for velocity was centered at 0 ± 120 ms and 30 ± 60 ms, for the center-out and obstacles tasks, respectively, consistent with an estimate of the current state of the arm. Note that, unlike for the movement angle, a nonstationarity exists in the speed profile (i.e., it is bell-shaped in time) for our task. Therefore, to generate the velocity OLT distributions, we first subtracted the surrogate TEFs from the actual velocity TEFs to control for any bias that might arise from this nonstationarity before computing the OLTs for velocity.

1. Paninski L, Fellows MR, Hatsopoulos NG, Donoghue JP (2004) Spatiotemporal tuning of motor cortical neurons for hand position and velocity. *J Neurophysiol* 91:515–532.
2. Bessou P, Emonetde. F, Laporte Y (1965) Motor fibres innervating extrafusal and intrafusal muscle fibres in cat. *J Physiol* 180:649–672.
3. Houk JC, Rymer WZ, Crago PE (1981) Dependence of dynamic-response of spindle receptors on muscle length and velocity. *J Neurophysiol* 46:143–166.
4. Matthews PBC (1972) *Mammalian Muscle Receptors and Their Central Actions* (Arnold, London).
5. Moran DW, Schwartz AB (1999) Motor cortical representation of speed and direction during reaching. *J Neurophysiol* 82:2676–2692.
6. Prochazka A, Gorassini M (1998) Models of ensemble firing of muscle spindle afferents recorded during normal locomotion in cats. *J Physiol* 507:277–291.
7. Schwartz AB, Kettner RE, Georgopoulos AP (1988) Primate motor cortex and free arm movements to visual targets in 3-dimensional space. 1. Relations between single cell discharge and direction of movement. *J Neurosci* 8:2913–2927.

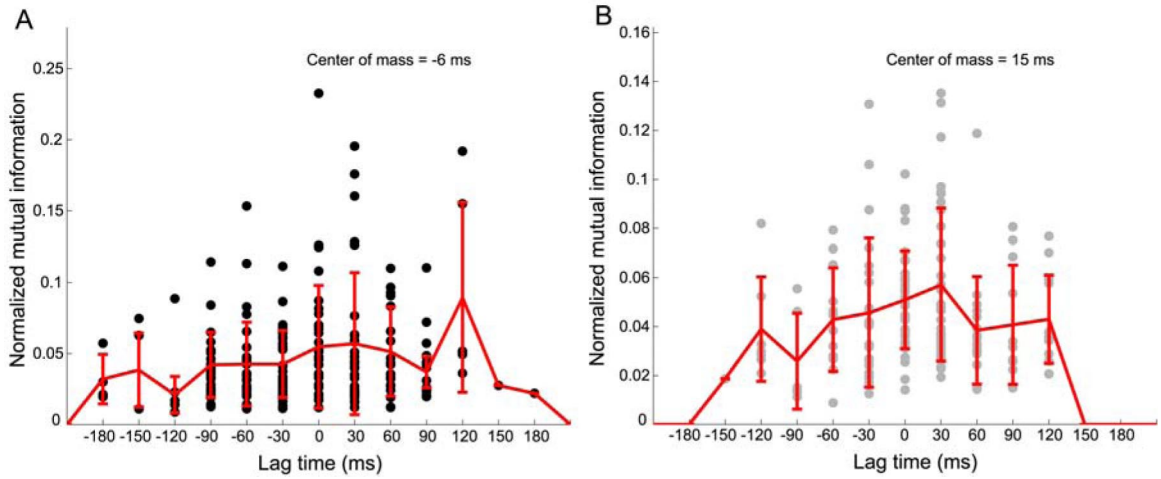

Fig. S1. Population summary of peak mutual information encoded at a neuron's OLT for the movement-angle population during center-out (*A*) and obstacle (*B*) tasks. Error bars represent SD of points at each OLT.

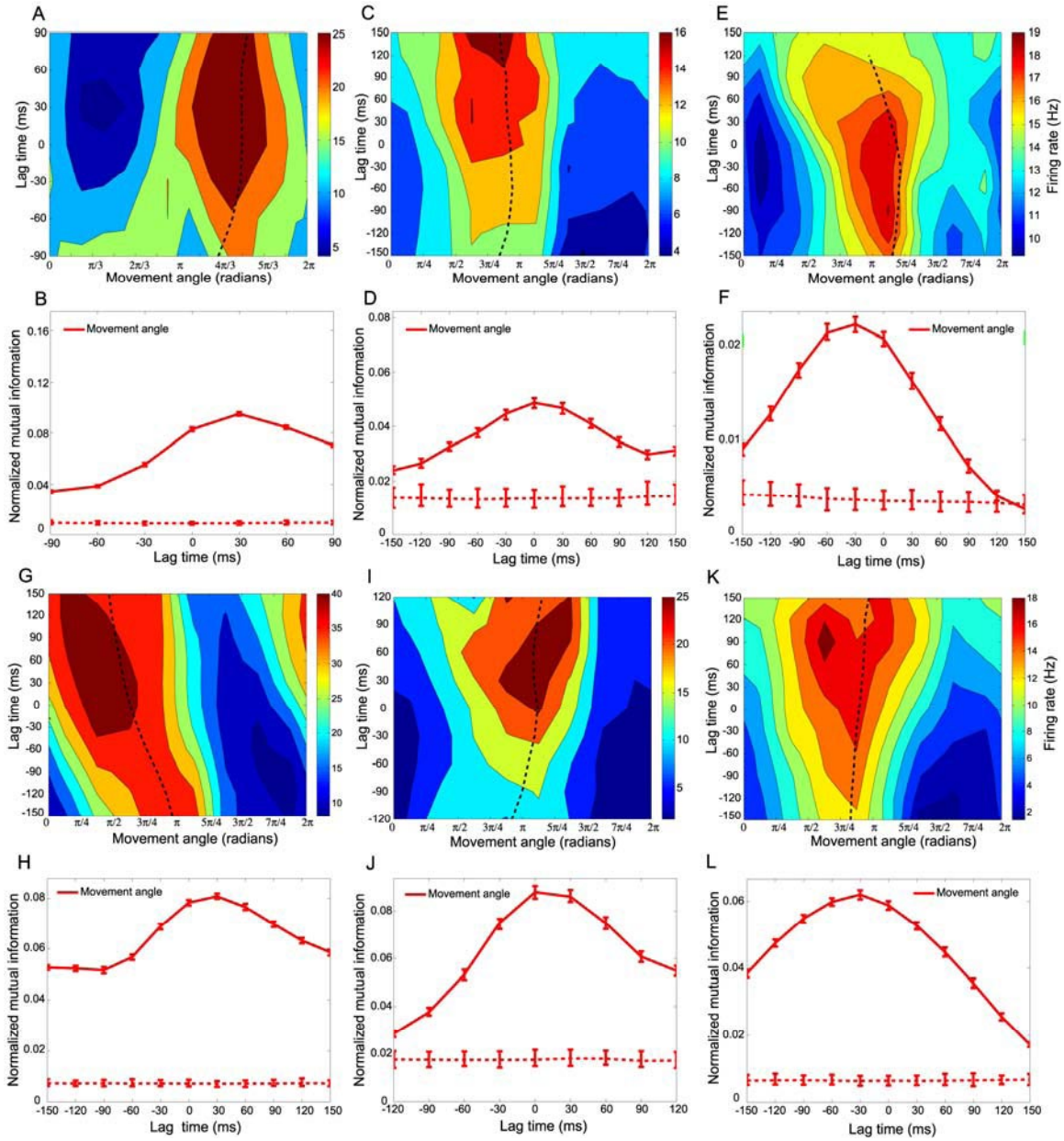

Fig. S2. Example STTFs and TEFs for neurons recorded during the obstacle task. Six STTF–TEF pairs (*A–B*, *C–D*, *E–F*, *G–H*, *I–J*, *K–L*) for neurons significantly tuned for movement angle.

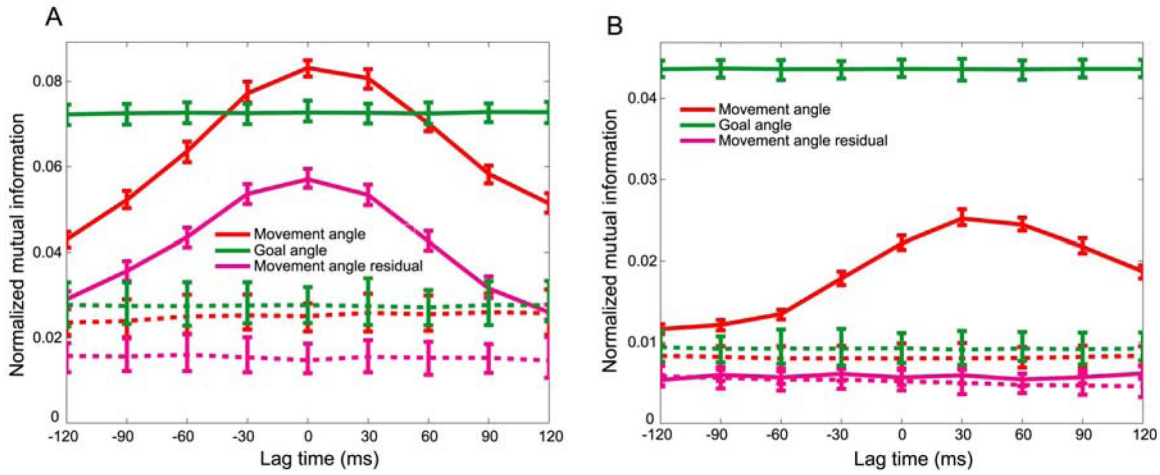

Fig. S3. Example residual movement-angle TEF plots. (*A*) The residual information is lower than the full movement-angle information but is still significantly above its residual noise level. Therefore, this cell significantly encoded the movement angle, independent of the goal angle. (*B*) A second example showing a cell that was no longer significantly tuned for movement angle after calculating the residual information.

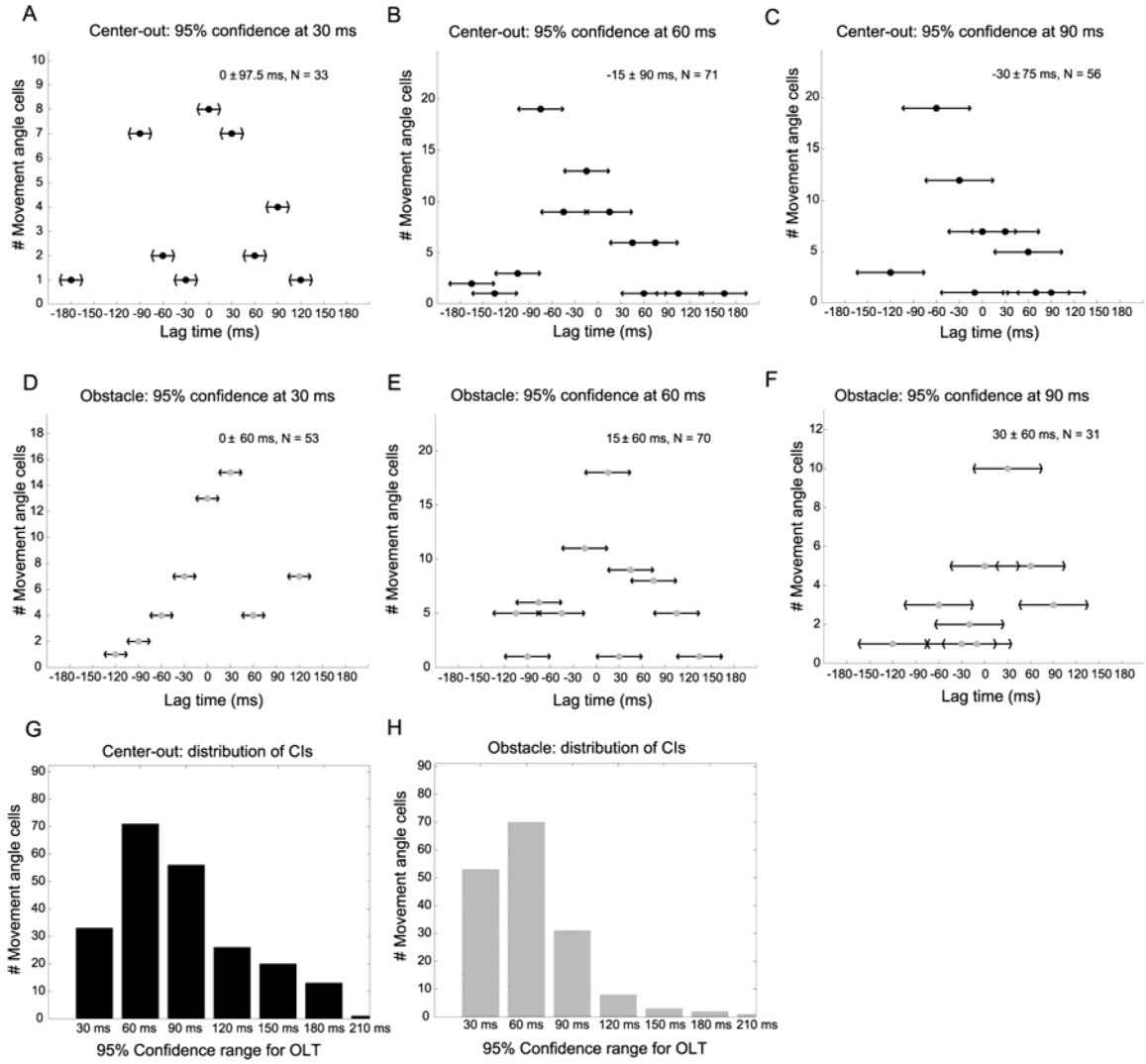

Fig. S4. Shown are 95% confidence intervals for OLT distribution. (*A–C*) Center-out OLT 95% confidence intervals are shown for cells for which the OLT is defined with 30 ms (*A*), 60 ms (*B*), and 90 ms (*C*) temporal precision. Extent of horizontal lines denotes the 95% confidence interval of the OLT. Filled dots represent the mean OLT for a given confidence interval. Text in the upper right-hand corner notes the median ± interquartile range OLT for each temporal precision plot. (*D–F*) Obstacle OLT confidence intervals plotted in the same format as *A–C*. Together, these plots suggest that the population best encodes the current state of cursor with varying degrees of temporal precision. (*G–H*) Seventy-eight percent and 93% of movement angle neurons had an OLT precision of 90 ms or less, using the 95% confidence criteria, for the center-out and obstacle tasks, respectively. The average temporal precision of OLT confidence intervals was smaller for the obstacle task (60 ± 60 ms, median ± IQR) than for the center-out task (90 ± 60 ms).